Proceedings of the ASME 2015 International Mechanical Engineering Congress and Exposition
IMECE2015
November 13-19, 2015, Houston, Texas

IMECE2015-50769

PHOTONICALLY SINTERED PZT ENERGY HARVESTER

Jing Ouyang
Rochester Institute of Technology
Microsystems Engineering
Rochester, NY, USA
jxo7115@rit.edu

Anirudh R. Penmetcha
Rochester Institute of Technology
Material Science and Engineering
Rochester, NY, USA
arp6270@rit.edu

Denis Cormier
Rochester Institute of Technology
Industrial and Systems Engineering
Rochester, NY, USA
drceie@rit.edu

David A. Borkholder
Rochester Institute of Technology
Microsystems Engineering
Rochester, NY, USA
david.borkholder@rit.edu

ABSTRACT

This paper reports an Aerosol-Jet printed micro scale Lead Zirconate Titanate (PZT) energy harvester directly sintered on a low melting point substrate in less than 1 msec using photonic sintering technology. To improve the output signal, d_{33} piezoelectric mode was employed by patterning silver electrodes as an interdigitated structure on top of a PZT film. The size of the device is 15.5 mm × 13.5 mm × 0.2 mm. Up to 2.4 V was measured at 145 MPa tensile bending stress level in the device after poling at 180 ℃ for 2 hours with an electric field of 30 kV/cm. Using an oscillating stress (~2.5 Hz) of approximately 145 MPa, the power as a function of load was determined by connecting the device with various series resistive loads. A maximal power of 0.1 μW was generated when driving into a 10 MΩ load. A PZT energy harvester, for the first time, is demonstrated which has been directly printed and sintered on a low melting temperature flexible substrate without a film transfer processes. This not only dramatically simplifies the fabrication process, but expands the possible substrate materials for PZT energy harvesters.

INTRODUCTION

Wearable devices, such as biological signal monitor [1, 2], gesture or facial expression recognizer [3, 4], and wearable computers [5, 6], have been intensively researched. In order to operate these devices, a power source that can provide stable, reliable and continuous energy is indispensable. While most devices use a battery, this requires routine recharging or replacement. There is an opportunity to leverage the mechanical energy from human body motion or the environment to power these devices. Lead Zirconate Titanate (PZT) is a commonly used piezoelectric material due to its high piezoelectric coefficient enabling generation of electrical energy in response to applied mechanical strain. To optimally scavenge human motion for power, the PZT should be fabricated on flexible and lightweight substrate materials that generally have a low melting point. Because of the mismatch of the PZT sintering temperature (> 800 ℃) and the melting point of the substrate (< 300 ℃), complicated PZT film transfer processes have traditionally been used to realize the desired device. For instance, Park et al. transferred a thermally sintered PZT film from sapphire to a polyethylene terephthalate (PET) substrate [7]. To avoid the complex transfer process, photonic sintering technology of thin PZT films with broadband, sub-msec, high intensity pulses was explored. Yamakawa, et al. recently used a hot plate at 350 ℃ to preheat the substrate in combination with a photonic flash lamp with an energy of 27 J/cm^2 to successfully sinter PZT film [8]. We adapted this approach to sinter our PZT film without substrate pre-heating. This eliminates the complicated PZT transfer processes. Instead the devices are directly processed on the low melting point flexible substrate.

DEVICE PREPARATION

The PZT ink composition is listed in Table 1 with weight percentage of each component. Commercially available PZT powders (APC 855, APC International Ltd., USA) with approximately 500 nm diameter size were mixed in the deionized water-Ethylene Glycol (Sigma-Aldrich Co. LLC, USA) solution. DisperBYK-180 (BYK Chemie, Germany) was added to disperse the PZT particles uniformly in the solvent.

Polyvinylpyrrolidone (Sigma-Aldrich Co. LLC, USA) was added to enhance the adhesion between the PZT and substrate following drying. The solution was stirred with a homogenizer (PRO 250, PRO Scientific Inc., USA) at a speed of 26000 rpm for 5 minutes to fully mix all the components. The prepared PZT ink was transferred to a 120 mL atomization jar in the Aerosol-Jet printer (Optomec, Inc., USA).

Table 1. PZT ink composition.

Material	Weight Percentage
PZT	30
DI water	49.6
Ethylene Glycol	12.4
DisperBYK 180	5
Polyvinylpyrrolidone	3

X-Ray Diffraction (XRD) on the PZT powders was carried out on a Rigaku D/MAX-2B Powder X-Ray Diffractometer (Rigaku Co., Japan) to investigate the crystalline structure of the PZT powders. The spectrum plotted in Fig. 1 is a representative of a strong perovskite phase in these PZT powders.

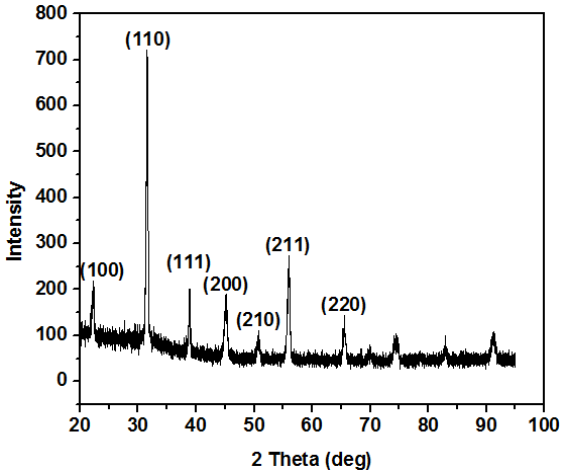

Figure 1. XRD spectrum of the commercially available PZT powders shows peaks characteristic of a highly crystalline perovskite structure.

The prepared PZT ink was Aerosol-Jet printed directly on a PET substrate (thickness = 80 μm). The Aerosol-Jet printer (Optomec, Inc., USA) is a maskless, CAD driven, non-contact printing system for controllably depositing nanoparticle inks. During printing, a mist created in the atomization jar was carried by nitrogen gas flow and transported to the ceramic printing nozzle head via tubing. In the nozzle head, the aerosol stream was focused and guided by a co-axial sheath gas (N_2) and finally deposited onto the substrate through a 200 μm diameter orifice forming a ~20-100 μm wide printed line, depending upon process parameters. The printing speed was controlled and fixed at 10 mm/s for the experiments, and the printing was repeated twice in the same region prior drying to enhance the particle density. The printed film was baked at 200 ℃ for 2 hours to remove solvent. The dried film was then photonically sintered with the PulseForge 3300 photonic sintering tool (Novacentrix Corporation, USA). This tool has a broadband (from ultraviolet to infrared) flash lamp that can controllably heat the printed nanoparticle films with high intensity, sub-millisecond pulses. The short pulse duration enables control of desired absorptive film heating and undesirable conductive substrate heating. This approach accordingly permits PZT sintering while minimizing substrate heating. The photonic energy was controlled by three parameters, namely applied voltage (450 V), pulse duration (270 μs) and number of pulses (N=1). This parameter combination gives 4086 mJ/cm^2 energy delivered to the film in less than 1 ms. The sintered film morphology was investigated under Scanning Electron Microscope (SEM) (JSM 6400, JEOL Ltd., Japan) and compared with the unsintered film as shown in Fig. 2.

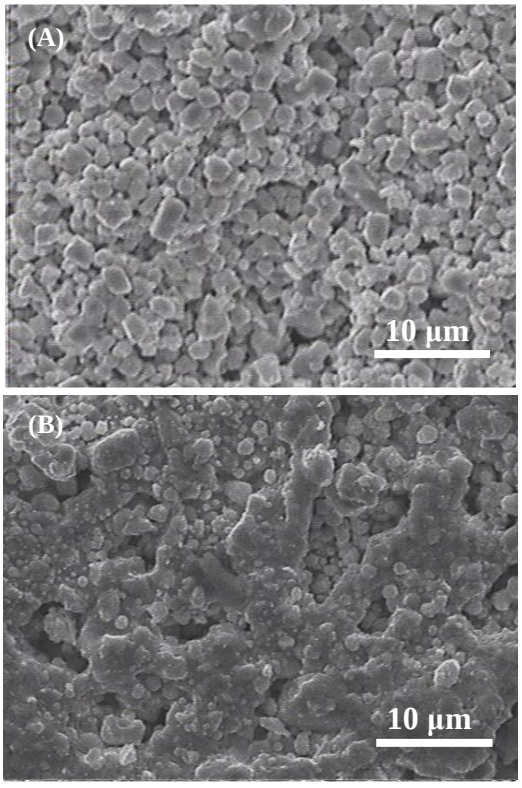

Figure 2. SEM images of PZT films. (A) Prior to sintering, the PZT powders were distributed uniformly in the film. (B) After photonic sintering, the powders fused and merged together.

It is noted that the PZT powders are uniformly but separately distributed in the dried PZT film shown in Fig. 2 (A). However, after photonic sintering, the connectivity between the individual particles had been significantly improved. Largely fused and merged particles are visible in Fig. 2 (B). Since the sintering process removes organic products from the film, the quantification of carbon (C) in the film can be an objective measure of photonic sintering quality. Energy-dispersive X-ray spectroscopy (EDS) spectra were captured in the SEM for

unsintered and sintered films as shown in Fig. 3. The photonically sintered PZT film has a very low C peak (approximately 20) compared with unsintered film (approximately 250). This low C content in the sintered PZT film is a strong indication that the organic products have been significantly removed from the PZT film during photonic sintering. The thickness of the PZT film before and after sintering was measured using a contact profilometer (P2, KLA Tencor, USA). The unsintered PZT film thickness of 43.3 μm was reduced during sintering to 18.7 μm due to removal of organic components and sintering densification of PZT particles.

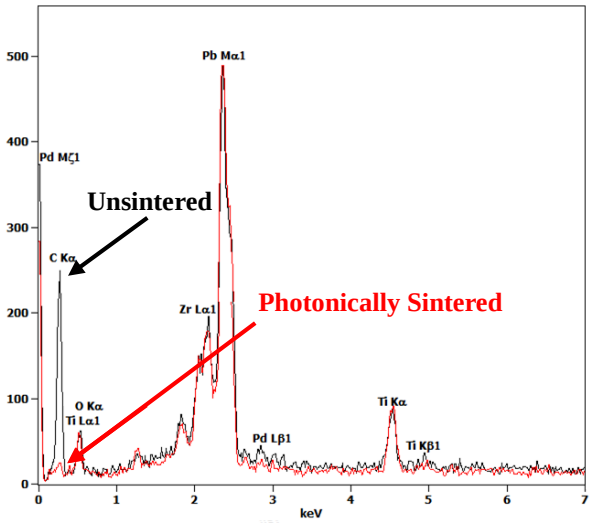

Figure 3. EDS results of unsintered (black) and photonically sintered (red) PZT films. The PZT film prior to sintering has a high C peak of approximately 250. Photonic sintering reduces the C peak to around 20. Low C content indicates the organic products have been removed from the PZT film during sintering.

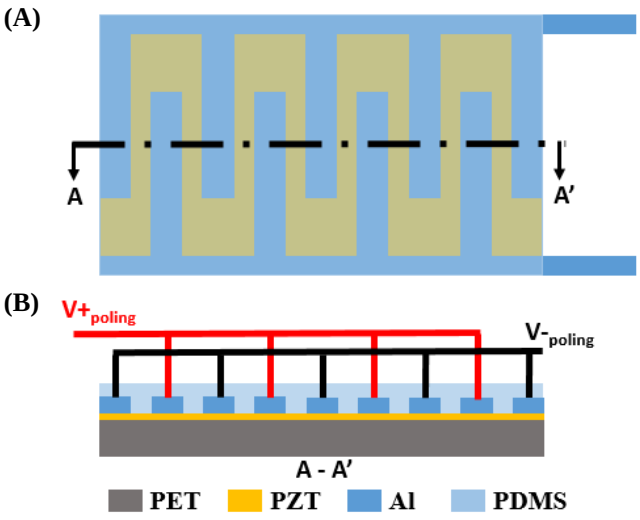

Figure 4. Schematic of top (A) and cross-sectional (B) views of the PZT energy harvester. The interdigitated electrode structure results in a poling direction parallel to the PZT surface.

Silver electrodes were patterned on top of PZT using an Ink-Jet printer (DMP-2831, FUJIFILM Dimatix, Inc., USA) and photonically sintered, as well. Since for PZT the d_{33} mode is approximately twice as large as the d_{31} mode [8], an interdigitated electrode structure was utilized to maximize the output signal obtained from the energy harvester. In order to protect the device, a layer of Polydimethylsiloxane (PDMS) (Dow Corning Co., USA) was coated the top surface. An illustration and optical image of the PZT energy harvester are shown in Fig. 4 and Fig. 5, respectively. The size (length × width × thickness) of the device was 15.5 mm × 13.5 mm × 0.2 mm. Silver epoxy (EJ2198, Epoxy Technology, Inc., USA) was used to connect the device to wires for poling and electric testing. The device was poled with an electric field of 30 kV/cm at 180 ℃ in atmospheric environment for 2 hours before piezoelectric characterization testing.

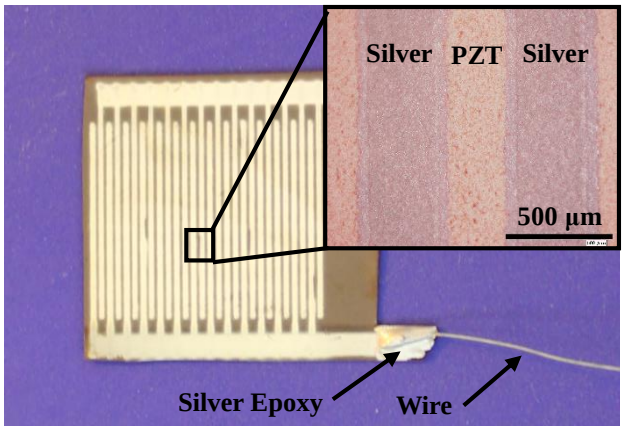

Figure 5. Optical image of the fabricated device (without coating PDMS layer). The PZT film was printed on transparent PET, and interdigitated silver electrodes were Ink-Jet printed on top of the PZT layer. The inset image shows the photonically sintered silver electrodes on the sintered PZT film.

FINITE ELEMENT SIMULATION

Mechanical finite element simulation was carried out in COMSOL 4.3a to study the stress induced in the PZT film when the energy harvester was deformed. The material parameters used in the simulation are listed in Table 2.

Table 2. Material parameters used in COMSOL simulations.

Parameters	Value	Unit
Young's modulus of PET	1.41×10^{10}	Pa
Poisson's ratio of PET	0.44	
Young's modulus of PZT	5.1×10^{10}	Pa
Poisson's ratio of PZT	0.3	
Young's modulus of PDMS	7.5×10^{5}	Pa
Poisson's ratio of PDMS	0.49	

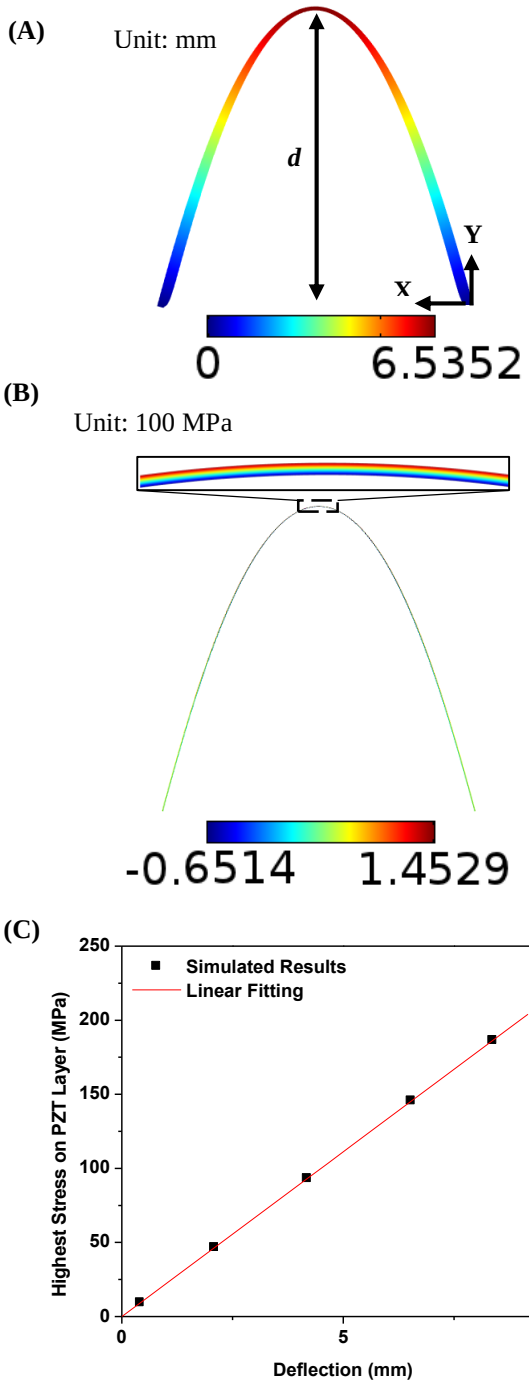

Figure 6. Mechanical finite element simulation results. Device deflection results in the positive y direction (A) with color indicating vertical displacement is 6.5 mm. The resulting stress in PZT film only is shown in (B) with the highest stress (145 MPa) at the location of greatest deflection. A linear relation between the highest tensile stress of the PZT layer and the deflection was obtained from the simulation (C). Based on this relation, the stress in the PZT film can be estimated by measuring the maximal deflection (*d*) of the device in the experiments.

The COMSOL simulation model was built as a PZT layer (thickness = 18.7 μm) sandwiched between the bottom PET layer (thickness = 80 μm) and top PDMS layer (thickness = 100 μm). In the experiment, a stage with one moving side (right) and one fixed side (left) was used to apply displacement to bend the device. Therefore, one end of the device was fixed (left) while the other end (right) translated in the x-axis compressing the device and inducing central flexure in the y-axis as shown in Fig. 6 (A). The resulting stress in the PZT layer was estimated (Fig. 6 (B)), with up to 145 MPa tensile stress at the location of greatest deflection (*d*). Notice the greatest tensile stress at the top surface and the greatest compressed stress at the bottom surface in the PZT are not equal. This is because the PZT is sandwiched in between PET and PDMS. However, PET is harder than PDMS. Therefore, the neutral axis (zero stress axis) of the entire device is not at the middle of the device thickness. Instead, it locates closer to the harder material (i.e. PET). The peak tensile stress increased linearly with *d* as shown in Fig. 6 (C). This result was used to estimate the tensile stress in PZT film based on measurement of the maximal deflection of the device (*d*).

PIEZOELECTRIC EXPERIMENTAL RESULTS

The piezoelectric response of the PZT energy harvester was characterized after poling by bending the device using a linear moving stage as shown in Fig. 7. An oscilloscope (TDS 2014B, Tektronix, Inc., USA) was used to record the output signal in all experiments. The position of the left side of the stage was fixed, with translation of the right side to induce flexure. The resulting open circuit voltage is plotted in Fig. 8, with the expected high-pass behavior.

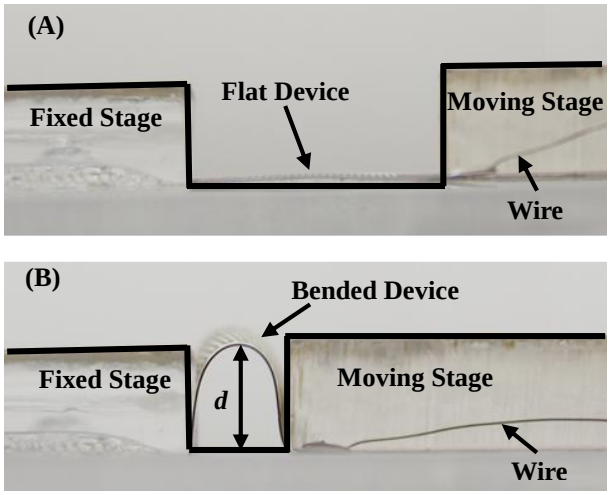

Figure 7. Photographs of the PZT energy harvester in the flat (A) and bended (B) states. The moving stages are highlighted with black lines for clarity. In this figure, the induced device deflection (*d*) was approximately 6.5 mm corresponding to approximately 145 MPa tensile stress at the greatest deflection location.

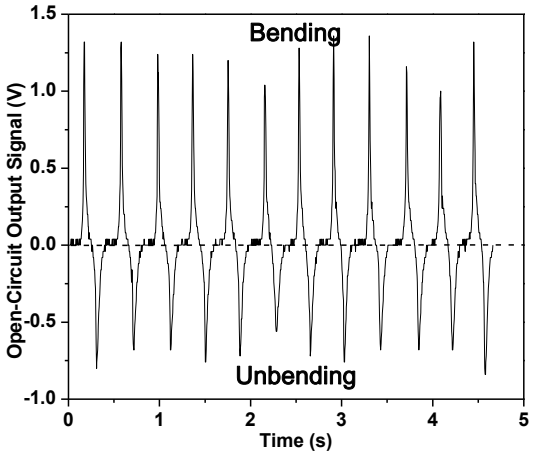

Figure 8. Open-circuit output signal in response to the reciprocated bending-unbending device deformation. Drive frequency was approximately 2.5 Hz. .

Based on the simulation result, the highest tensile stress on the PZT layer was estimated by measuring the maximal deflection (*d*) of the device via ImageJ. The output open-circuit voltage corresponding to the peak tensile stress from the PZT film is shown in Fig. 9, with a positive linear relation between the output signal and stress obtained (R^2 = 0.88). The greatest voltage obtained was 2.4 V with an applied stress of approximately 145 MPa.

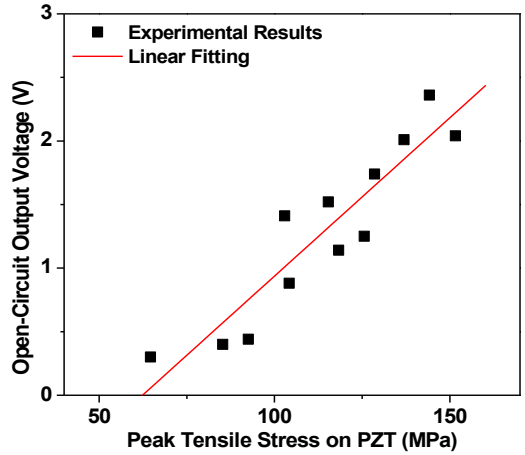

Figure 9. Open-circuit output voltage increases linearly with induced stress in the PZT film. Up to 2.4V was obtained with an applied stress of 145 MPa.

Capacitance (C_{EH}) of the PZT energy harvester was measured using a simple RC circuit to analytically determine the optimal load impedance (*Z*). A 10 kΩ resistor was connected with the device in series. A square wave generated from a signal generator (33120A, Agilent Technologies, USA) with 10 Hz frequency drove the circuit. The measured time constant (τ) of this RC circuit was approximately 60 μs. Therefore, the C_{EH} of the energy harvester can be calculated as 6 nF via Eq. 1

$$\tau = RC_{EH} \quad (1)$$

where *R* equals 10 kΩ. The load impedance for maximum power transferred from energy harvester to the load can be estimated by Eq. 2 [9]

$$Z = \frac{1}{2\pi f C_{EH}} \quad (2)$$

where *f* is the driving frequency (i.e. 2.5 Hz in this experiment). Therefore, the calculated load impedance for maximal power is 10.6 MΩ

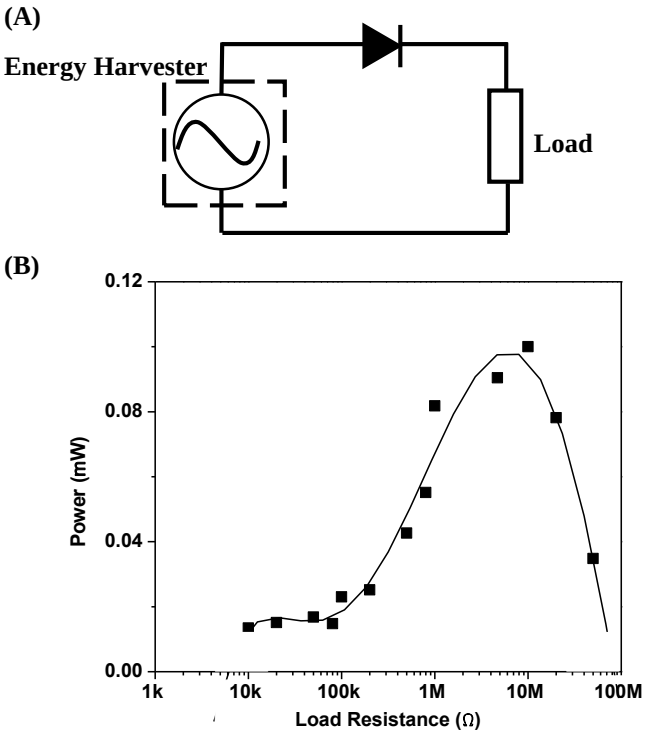

Figure 10. (A) Rectifying circuit for the PZT energy harvester used for determination of power delivered to different load resistors. (B) The measured output power delivered to different load resistances ranging from 10 kΩ to 50 MΩ with a peak stress of approximately 145 MPa. The output power is gradually building up with resistance increase. Up to 0.1 μW was generated when the energy harvester was connected to a 10 MΩ load.

To investigate the effective power output of the PZT energy harvester, the device was connected with various series resistive loads ranging from 10 kΩ to 50 MΩ with a fixed stress of approximately 145 MPa (corresponding to about 6.5 mm deflection) using a rectifying circuit shown in Fig. 10 (A). By measuring the voltage signal on load, the power can be calculated by Eq. 3.

$$P = \frac{V^2}{R} \quad (3)$$

where *V* is the RMS (Root Mean Square) value of the measured voltage signal on load. *R* is resistance of the load. *P* is the power generated from PZT energy harvester. The experimental results are plotted in Fig. 10 (B).

Consequently, 0.1 μW was generated when connected the PZT energy harvester to a 10 MΩ load. This matches well to the analytical load impedance result and has approximately equal performance to the proposed flexible PZT energy harvesters by Wu et al [10] (0.12 μW). However, it is lower than the device reported by Park et al [7] (12.25 μW). The possible reasons are: firstly, lower poling field was used in our experiment (30 kV/cm versus 100 kV/cm used in Park's work); secondly, the sintering energy was not high enough to penetrate the entire PZT film, resulting in weak sintering at the interface of the PZT and PET. Increasing the poling electric field strength, and optimizing the sintering parameters to achieve a superior sintered film offer opportunities to significantly improve piezoelectric performance. Moreover, the ink-jet printed electrodes width has a variation of approximately 80 μm, which limited the sintering electric field to low strength. Using other electrodes patterning technology, such as photolithography and etch process [11], lift-off process [12] or microstamping [13], would achieve more uniform electrode width and further enhance the poling process and piezoelectric performance.

CONCLUSION

This paper, for the first time, reports an Aerosol-Jet printed PZT energy harvester directly sintered on a low melting point substrate using photonic sintering technology in less than 1 millisecond. Interdigitated silver electrodes were Ink-Jet printed on top of the PZT film to leverage the more sensitive d_{33} mode to improve the output signal. The piezoelectric response was characterized by bending the device with the expected linear relation between open-circuit output voltage and applied stress obtained. Up to 2.4 V was measured at 145 MPa stress level. Using a fixed stress of approximately 145 MPa, the power versus load was determined by connecting the device with various series resistive loads. Higher power can be generated while connected with larger loads. Up to 0.1μW was obtained while connected to a 10 MΩ load. Photonic sintering technology avoids complicated PZT transfer process to low melting and flexible substrate. Consequently, it dramatically expands the possible substrate materials for PZT energy harvesters and shortens the fabrication time.

.

ACKNOLEDGEMENTS

The authors thank Prof. S. A. Williams from Chemistry and Materials Sciences, RIT, for discussion of the formula of the PZT ink; Prof. R. K. Hailstone from Imaging Science, RIT, for obtaining the SEM images and EDS plots; and Prof. S. K. Gupta from Mechanical Engineering, RIT, for assistance with the XRD spectrum. This project was supported by the National Science Foundation grant IIP-1237761.

REFERENCES

[1] Winokur, E. S., Delano, M. K., and Sodini, C. G., 2013, "A Wearable Cardiac Monitor for Long-Term Data Acquisition and Analysis," IEEE Trans. Biomed. Eng., 60(1), pp. 189-192.

[2] Rienzo, M. D., Rizzo, F., Parati, G., Brambilla, G., Ferratini, M., and Castiglioni, P., 2005, "MagIC System: a New Textile-Based Wearable Device for Biological Signal Monitoring. Applicability in Daily Life and Clinical Setting," Proc. 27th Ann. Int. IEEE EMBS Conf., Shanghai, China, pp. 7167–7169.

[3] Scheirer, J., Fernandez, R., and Picard, R. W., 1999, "Expression Glasses: A Wearable Device for Facial Expression Recognition," Proc. of CHI 1999, Human Factors in Computer Systems, Pittsburgh, PA.

[4] Starner, T., Weaver, J., and Pentland, A., 1997, "A Wearable Computer Based American Sign Language Recognizer," Proc. IEEE Int. Symp. Wearable Computing, pp. 130-137.

[5] Smailagic, A., Siewiorek, D., and Reilly, D., 2001 "CMU Wearable Computers for Real-Time Speech Translation," IEEE Personal Communications, 8(2), pp. 6-12.

[6] Bai, Y., Li, C., Yue, Y., Jia, W., Li, J., Mao, Z. H., and Sun, M., 2012, "Designing a Wearable Computer for Lifestyle Evaluation," Bioengineering Conf. (NEBEC), 2012 38th Annual Northeast, Philadelphia, PA, pp. 93-94.

[7] Park, K. I., Son, J. H., Hwang, G. T., Jeong, C. K., Ryu, J., Koo, M., Choi, I., Lee, S. H., Byun, M., Wang, Z. L., Lee, J. K., 2014, "Highly-Efficient, Flexible Piezoelectric PZT Thin Films Nanogenerator on Plastic Substrates," Adv. Mater., 26(16), pp. 2514-2520.

[8] Yamakawa, K., Imai, K., Arisumi, O., Arikado, T., Yoshioka, M., Owada, T., and Okumura, K., 2002, "Novel Pb(Ti, Zr)O_3 (PZT) Crystallization Technique Using Flash Lamp for Ferroelectric RAM (FeRAM) Embedded LSIs and One Transistor Type FeRAM Devices," Jpn. J. Appl. Phys., 41 (4B), pp. 2630-2634.

[9] Park, J. C., Lee, D. H., Park, J. Y., Chang, Y. S., and Lee, Y. P., 2009, "High Performance Piezoelectric MEMS Energy Harvester Based on D33 Mode of PZT Thin Film on Buffer Layer with $PbTiO_3$ Inter Layer," Proc. Int. Solid State Sens., Actuators, Microsyst. Conf., TRANSDUCERS, Denver, CO, pp. 517-520.

[10] Wu, W., Bai, S., Yuan, M., Qin, Y., Wang, Z. L., and Jing, T., 2012, "Lead Zirconate Titanate Nanowire Textile Nanogenerator for Wearable Energy-Harvesting and Self-Powered Devices," ACS Nano, 6(7), pp. 6231-6235.

[11] Yu, H. G., Zou, L., Deng, K., Wolf, R., Tadigadapa, S., and Mckinstry, S. T-., 2003, "Lead Zirconate Titanate MEMS Accelerometer Using Interdigitated Electrodes," Sens. Actuators A, 107 (1), pp. 26-35.

[12] Jeon, Y. B., Sood, R., Jeong, J. –H., and Kim, S. –G. 2005, "MEMS Power Generator with Transverse Mode Thin Film PZT," Sens. Actuators A, 122 (1), pp. 16-22.

[13] Takakuwa, A., Ikawa, M., Fujita, M., and Yase, K., 2007, "Micropatterning of Electrodes by Microcontact Printing Method and Application to Thin Film Transistor Devices," Jpn. J. Appl. Phys., 46 (9A), pp. 5960-5963.